Physics – Uspekhi **66** (7) 691 – 703 (2023)

REVIEWS OF TOPICAL PROBLEMS PACS number: **96.60.–j**

Subsecond pulses in microwave emission from the Sun

A T Altyntsev, N S Meshalkina, S V Lesovoi, D A Zhdanov

DOI: https://doi.org/10.3367/UFNe.2022.06.039205

Contents

1. **Introduction** 691
2. **Mechanisms of emission and propagation effects** 692
3. **Instruments for studying the spatial characteristics of subsecond pulses** 693
4. **Observation data on subsecond pulses** 695
   4.1 Dependence of source sizes on the position on the disk; 4.2 Effects of radiation reflection from the solar atmosphere underlayers; 4.3 Polarization properties; 4.4 Spectral characteristics of subsecond pulses
5. **Discussion of results and prospects of studies of microwave subsecond pulses** 702

References 703

Abstract. The current state of research on microwave subsecond pulses (SSPs) based on observations of radio-frequency radiation from solar flares with high temporal, spatial, and spectral resolutions is reviewed. It is shown that knowledge about the localization of SSP sources in the flare region, available with the help of large radio interferometers, radically affects the understanding of the nature of SSPs. Based on the unique observational material accumulated in radio observations over the past 30 years, the characteristics of SSPs have been studied, they have been classified according to their spectral characteristics, and the mechanisms of their generation have been determined.

Keywords: radio emission, microwave bursts, fine temporal structure

1. Introduction

Interest in the study of solar activity processes is related to both the growing requirements for the forecast of geoeffective phenomena and a number of fundamental problems of plasma physics, since the solar atmosphere is a natural laboratory that allows studying under natural conditions the phenomena occurring in the stars unavailable to laboratory studies. The processes studied by solar physics are also observed in other astrophysical objects. The possibility of studying their characteristics with high space and time resolution allows solving problems at an unprecedented level of minuteness and reliability compared to far astrophysical objects. Knowledge of the universal physical processes obtained in solar studies allows checking and specifying the hypotheses, theory, and models of astrophysical objects. The applied significance of studying the Sun is also great, as it is the most important cosmic factor affecting Earth's climate, technology, infrastructure, and life activity of humanity.

The processes of solar activity due to the release of deeply located magnetic fields occur in the solar atmosphere in an extremely wide range of energy, time, and space scales. This review is devoted to studies of a phenomenon, particular but extreme in its characteristics, subsecond radio bursts, recorded, as a rule, during solar flares. Solar flares are one of the most powerful manifestations of the Sun's activity, significant for geophysical processes. Radio observations are the most sensitive method of detecting nonthermal electrons in the rarefied plasma of the solar corona.

The existence of fine time structure in the radio emission of solar flares has been known for a few decades. Observations in the meter and decimeter ranges were the first to become available at selected frequencies. The meter-range radiometers with millisecond time resolution that appeared in the 1960s recorded the most short-term manifestations of solar activity. Subsecond pulses (SSPs) — intense pulses of radiation with a duration of less than 1 s, which, as a rule, appeared against the background of a longer burst — were the first to draw attention. The discovery of SSP clusters was considered a confirmation of the popular hypothesis about flare energy release as an aggregation of elementary particle acceleration events [1, 2].

SSPs are observed in all ranges of radio emission of flares; however, the frequency of their recording depends on the radio emission range. In the meter range at frequencies below 300 MHz, clusters of a few thousand SSPs at intervals of tens of seconds are generated during flares in the upper corona. In the decimeter range (up to 3 GHz), SSPs are emitted by beams of electrons propagating in flare loops. In this review, we discuss studies of bursts with a fine temporal structure in the microwave (centimeter) range (frequencies above 3 GHz), whose sources are located near the sites of primary energy release in the flares, where electrons are accelerated, and in low flare loops. At these frequencies, observations with high

A T Altyntsev [a], **N S Meshalkina** [b], **S V Lesovoi** [c], **D A Zhdanov** [d]
Institute of Solar-Terrestrial Physics,
Siberian Branch of the Russian Academy of Sciences,
ul. Lermontova 126a, 664033 Irkutsk, Russian Federation
E-mail: [a] altyntsev@iszf.irk.ru, [b] mtssnami@yandex.ru,
[c] lesovoi@iszf.irk.ru, [d] zhdanov@iszf.irk.ru

Received 16 November 2021, revised 18 May 2022
Uspekhi Fizicheskikh Nauk **193** (7) 737 – 750 (2023)
Translated by V L Derbov

spatial resolution were available. In the above range, SSPs are recorded in about 10% of flares in series of a few bursts per flare. In some events, the number of SSPs reaches a few tens at intervals of up to 1 min. Later, it became possible to observe the dynamic spectra of solar flares. It turned out that the dynamic spectra in the case of fine temporal structure are distinguished by a variety of shapes; in particular, observed are bursts with frequency drift (type III), bursts with complex frequency drift (U and N types), 'zebra' structures, and spikes (narrow-band driftless bursts). The results of observations of the fine spectral structure in various ranges were summarized in reviews [1–4].

It was found that the bursts with a narrow instantaneous radiation band are generated by plasma turbulence excited by the nonequilibrium plasma in the flare region. The SSP radiation frequencies are close to the fundamental (cyclotron of Langmuir) plasma frequencies or their harmonics in the source. The narrow radiation band in some events, to a few percent of the mean, implies a small size of the source as compared to the scales of magnetic field or plasma density variation in the SSP emission region.

The corresponding estimates show that the size of the SSP radiation sources should not exceed a few hundred kilometers. To produce the observed fluxes greater than a few solar flux units (sfu),[1] the brightness temperature of the source should be anomalously high (up to 10^{15} K), which exceeds the plasma temperature and the kinetic energies of the emitting particles by orders of magnitude. These properties stimulated interest in SSPs as the shortest-term and highest-power pulses of radiation in the solar atmosphere.

High-power bursts of millisecond duration were recorded from galactic and extragalactic sources (see, e.g., [5]). The brightness temperatures of rapid radio bursts can reach 10^{33} K and certainly have a coherent origin of radiation. The study of emission mechanisms of subsecond microwave bursts on the Sun allows determining the plasma parameters in the sources of millisecond pulses, unavailable for measuring in far astrophysical sources.

To verify the SSP generation mechanism and, consequently, to realize the diagnostic potential of SSP observations, in is necessary to know the parameters of plasma in the sources. This problem is solvable by means of radio observations with high enough spatial resolution, making it possible to localize the SSP sources relative to the flare sources in the optical, ultraviolet, and X-ray ranges. Supplementing the microwave data with observations in other ranges allows determining the plasma parameters at the site of SSP generation.

Solving the problem of SSP source localization in the flare region is possible in the microwave range, where a high enough spatial resolution of a few arc seconds can be achieved at a reasonable telescope aperture size of a few hundred meters. In the microwave range, the main morphological SSP types are recorded, characteristic of the decimeter and meter ranges. Particular interest in the observation of SSP sources in the centimeter range is due to their closeness to the sites of primary flare energy release and, therefore, the possibility of extracting information on the plasma density and magnetic field magnitude at the sites of acceleration of electrons. On the other hand, the small dimensions of SSP sources allow using them as point sources in studying the effects of electromagnetic wave propagation in the lower solar corona and the characteristics of large-scale plasma density fluctuations in the upper corona. It turns out that the visible dimensions of SSP sources can be of the order of 10 arc seconds and depend on their position on the Sun disk. The reasons for and consequences of this are discussed in Section 4.1.

In spectrometric observations, it was established that the probability of the appearance of subsecond structures in flare radiation decreases with an increase in frequency [1]. At the reception frequency of a radio telescope, a statistically significant number of narrow-band SSP events (a few tens) can be recorded only during a long time of the order of the solar cycle. Therefore, significant statistics can be accumulated in observations only using radio telescopes with subsecond resolution, the observation daytime of which is practically completely devoted to the Sun. For the broad reception band of spectropolarimeters, the proportion of fine-structured flares considerably increases, which testifies to the narrow band of radiation in most SSPs. In one of the latest statistical studies, it was shown that in the band of 4–8 GHz SSPs are observed in almost half of the flare events [6].

The observation of radio bursts with large interferometers with subsecond time resolution became possible in the 1990s. The first publication [7] described the SSP observation recorded at a frequency of 2.8 GHz with a two-element interferometer. Analyses of observations have shown that the SSP source was observed on the Sun disk section crossing a solar spot with a high magnetic field. Therefore, the observations were interpreted by the authors in favor of the maser mechanism of SSP generation on cyclotron harmonics. A few more papers describing individual cases of recording SSPs with the interferometers WSRT (Netherlands) [8], Nobeyama (Japan) [9], and Westerbork (Netherlands) [10] were published in the 1990s.

The present review discusses the results of systematic studies of bursts with fine temporal structure in the microwave (centimeter) range based mainly on the observations of SSPs with spatial resolution using unique radio telescopes: the Siberian Solar Radio Telescope (SSRT, 5.7 GHz) and Nobeyama Radioheliograph (NoRH, 17 and 34 GHz). Their relatively close geographical position and subsecond time resolution allowed conducing synchronous observations of SSPs during solar flares.

2. Mechanisms of emission and propagation effects

Before proceeding to a discussion of the SSP observation results, we briefly dwell on the main mechanisms of their generation, proposed by theory. In dynamic spectra, two groups of structures are distinguished: broadband pulses with the radiation range $\Delta f/f \geqslant 1$ and bursts with the instantaneous radiation band smaller by an order of magnitude, $\Delta f/f \leqslant 0.1$.

In the case of broadband SSPs generated in individual elementary events of energy release, they are interpreted within the gyrosynchrotron radiation generated by short-time pulses of relativistic electrons with energies up to ~ 1 MeV, propagating in the magnetized plasma of flare loops [11–13]. Such radiation is incoherent, i.e., each electron radiates independently of others, and the total emission of the source is obtained by summation over the distribution of the emitting electrons. The brightness temperature of gyrosyn-

[1] 10^{-22} W m^{-2} Hz^{-1}.

chrotron sources is limited by the kinetic energy of emitting electrons and inverse Compton scattering.

The brightness temperature of SSP sources with a narrow instantaneous radiation band can exceed the brightness of thermal and gyrosynchrotron sources by many orders of magnitude, since the radiation has a coherent nature [12]. In the solar corona, the coherent mechanisms are related to the excitation of some plasma instabilities at frequencies close to the plasma or cyclotron frequency or their harmonics [1, 2]. If the SSP radiation frequency is related to the plasma one, i.e., the local Langmuir frequency

$$f_{\rm pe} = \frac{1}{2\pi}\sqrt{\frac{4\pi n e^2}{m}}, \qquad (1)$$

where n is the plasma concentration, e is the electron charge, and m is the electron mass, then the mechanism of the radiation is identified as 'plasma radiation.' In this case, the radiation is generated as a result of phased collective plasma disturbances. The second mechanism, the electron-cyclotron maser (ECM) one, generates radiation near the cyclotron frequency:

$$f_{\rm ce} = \frac{1}{2\pi}\frac{eB}{\gamma mc}, \qquad (2)$$

where B is the magnetic field, γ is the Lorentz factor, and c is the speed of light.

In the theory of plasma radiation, three processes are distinguished: (a) the excitation of Langmuir turbulence by some plasma instability; (b) the generation of electromagnetic radiation at the fundamental frequency (close to the plasma one) upon the scattering of longitudinal plasma waves by fluctuations related to plasma ions; (c) the generation of transverse electromagnetic waves at a harmonic of the fundamental frequency, i.e., close to the double Langmuir frequency, appearing upon the coalescence of two plasma waves.

It should be noted that if the SSP radiation is generated at frequencies close to the Langmuir frequency, then the absorption of the radiation by Coulomb collisions in the vicinity of the source is critical for the possibility of recording it on Earth. This effect was reported for the first time in Ref. [14]. The free-free absorption in the plasma surrounding the source reduces the observed radiation by the factor $\exp(-\tau)$,

$$\tau = \left\{ \begin{array}{c} 46 \\ 1.2 \end{array} \right\} T\,[\mathrm{K}]^{-3/2} f^2\,[\mathrm{GHz}]\, H\,[\mathrm{cm}], \qquad (3)$$

where the upper number in curly brackets is an estimate for a wave at the fundamental frequency and the lower one relates to a harmonic, and H is the scale of density change on the path of radiation propagation. At a temperature of 1 MK at a frequency of 5.6 GHz, $\tau \approx 1$ at $H = 7$ km for the fundamental plasma frequency and at $H = 280$ km for the second harmonic. The absorption rapidly increases with an increase in frequency, which explains rare observation of SSPs in the microwave range. In particular, favorable conditions for radiation release can be implemented across flare loops with a sharp gradient of plasma density at the boundary. Note that, when propagating a few optical thicknesses in the solar corona, the collimation of radiation occurs and a change in the SSP circular polarization degree is possible, since the coefficient of collisional absorption depends on whether the wave is ordinary or extraordinary.

The conditions for ECM generation of an SSP in the lower corona are tougher, since the gyromagnetic radiation is modified by the presence of plasma. In plasma with $f_{\rm pe} > sf_{\rm ce}$, the cyclotron radiation at the sth harmonic cannot leave the source. Cyclotron radiation at the fundamental frequency is possible in principle only at $f_{\rm pe} < f_{\rm ce}$, and the dispersion of waves in the plasma additionally restricts the condition of effective radiation to $f_{\rm pe} \ll f_{\rm ce}$ [13]. This condition, as a rule, does not hold in the lower corona, where the SSP sources are located.

Measurements of the duration and size of SSP sources can be substantially affected by the scattering of electromagnetic radiation by plasma inhomogeneities in the solar corona. Theoretical estimates of the scattering that leads to an increase in the visible size of sources and broadening of pulses in time have been obtained for the microwave range in Refs [15, 16].

3. Instruments for studying the spatial characteristics of subsecond pulses

The main instrument to carry out the program of microwave SSP observations was the Siberian Solar Radio Telescope (SSRT) [17]. Observations with subsecond time resolution were performed from July 1992 to June 2013. The SSRT was located in the Tunkinsky District of Buryatia and allowed recording solar microwave bursts in the one-dimensional regime at a frequency of about 5.7 GHz with a time resolution of 14 ms and space resolution of 15″. When constructing two-dimensional images, the time resolution was only 2–3 min, but the maps were useful in the analysis of one-dimensional distributions (frequency scans).

The SSRT was a cross-shaped interferometer with antenna arrays oriented along the north–south (N–S) and east–west (E–W) directions. The interferometer consisted of 256 antennas 2.5 m in diameter, with the edge antennas separated by a distance of 622 m. Continuous observations of the Sun were carried out for 6 – 10 hours daily, depending on the season.

To investigate the SSP sources, one-dimensional distributions of radio brightness in intensity and circular polarization (frequency scans) were used, which were recorded each 14 ms simultaneously by the east–west and north–south antenna arrays. Sweeping the scan over the solar disk was implemented using a multichannel spectrometer in the frequency band of 120 MHz.

Figure 1 shows an example of the typical subsecond pulses observed. In the time profiles of intensity and circular polarization, a few pulses are distinguished with a duration of ~ 150 ms. In this case, the SSP radiation is right-hand polarized at a degree of up to 50%.

Figure 1b shows a sequence of segments of scans with a flare recorded by the north–south array of antennas. The horizontal dashed line marks the position of the brightness center of the continual solar burst. Bright spots, the response to SSPs, are displaced by 40″. Their position is marked by a solid line. Figure 1c presents the dynamic spectrum in the range of 5.2–7.6 GHz measured by Chinese spectropolarimeters, including the SSRT reception band (between the dashed lines). From the dynamic spectrum, it follows that the subsecond pulses observed at the SSRT temporal profiles are a response to narrow-band drifting bursts [18].

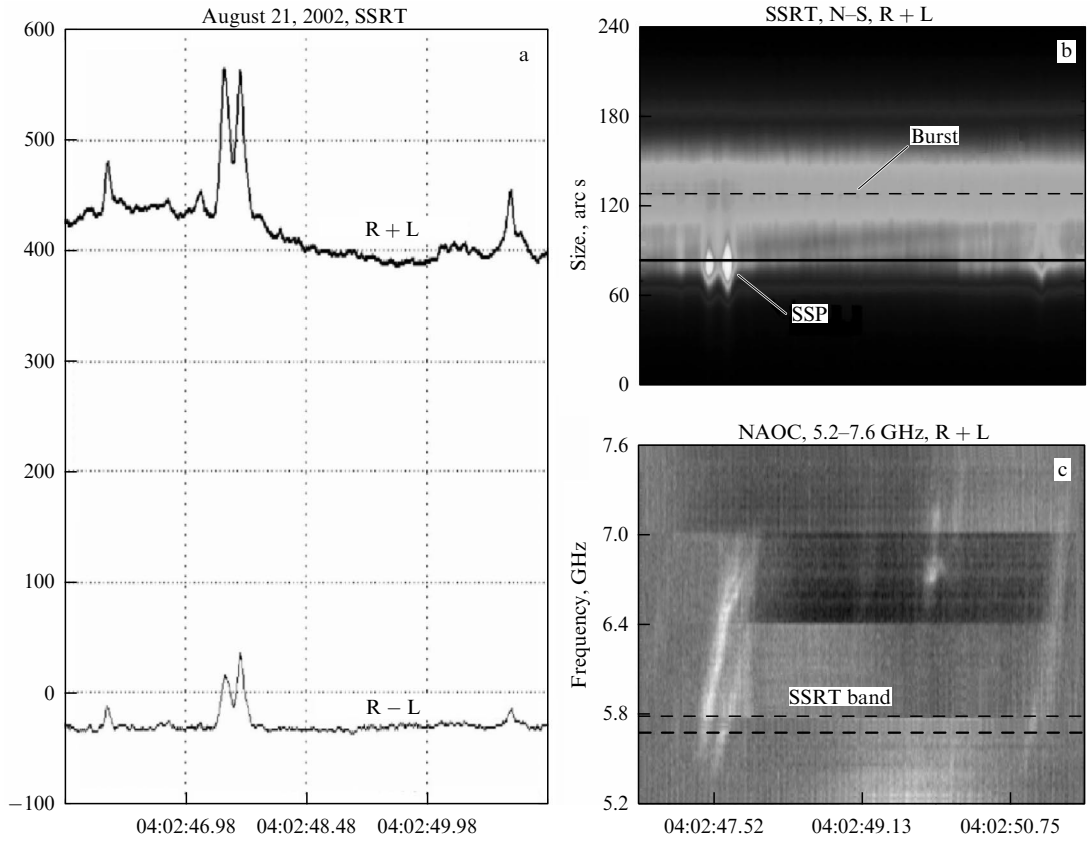

Figure 1. August 21, 2002. (a) Profiles of I and V Stokes parameters, obtained at the SSRT at a frequency of 5.7 GHz; R — right-hand circular polarization, L — left-hand circular polarization. (b) Time base of SSRT one-dimensional scans. Dashed horizontal line marks the position of the burst maximum, solid horizontal line marks the maximum of the subsecond pulse. (c) NAOC dynamic spectrum. Dashed horizontal lines mark the SSRT reception band.

The technique of analyzing one-dimensional images of the Sun is described in papers by Altyntsev et al. [19–22]. The reception system of the SSRT is a spectrum analyzer in the frequency band of 120 MHz. For this purpose, an acousto-optic receiver with 250 frequency channels was used, each corresponding to a fan of knife-edge directional patterns. The bandwidth of one frequency channel is 0.48 MHz. The response at each frequency corresponds to the emission from a narrow strip on the solar disk, the position and width of which depend on the observation time, type of antenna array, and frequency. The signals from all frequency channels are simultaneously recorded and generate a one-dimensional distribution (scan) of the solar radio brightness every 14 ms. In this case, the spatial resolution is determined by the width of the directional pattern of the 1D antenna array at a given local time [18].

From August 2010, in the Badary Radio Astronomical Observatory of the Institute of Solar-Terrestrial Physics, Siberian Branch of the Russian Academy of Sciences, regular observations of subsecond bursts began to be conducted on the Badary Broadband Microwave Spectropolarimeter (BBMS) [6]. The received bandwidth covered 3.8–8.2 GHz. The spectral resolution of the instrument was 120–150 MHz. The temporal resolution of the stored data was 10 ms at a flux sensitivity of about 1 sfu. The observation data are time dependences of the integral fluxes at 26 frequencies in both circular polarizations.

Important observations for the program of SSP studies were carried out at the National Astronomical Observatory of Japan located 120 km west of Tokyo. The Nobeyama Radioheliograph (NoRH) [23] of the parallel aperture synthesis obtained images of the Sun disk in brightness temperatures at frequencies of 17 and 34 GHz with a spatial resolution to 10″ at 17 GHz and time resolution of 1 s in routine observations. When observing short-term events, the time resolution was 50 ms before 1995 and 100 ms after 1995. The Nobeyama Radiopolarimeters (NoRPs) [24–26] recorded the integral solar flux at frequencies of 1, 2, 3.75, 9.4, 17, 35, and 80 GHz with a temporal resolution of 1 s in the routine mode and 0.1 s in the flare mode. The observations with the NoRH were carried out daily from 21:30 to 06:30 UT and were simultaneous with the SSRT for 4–5 h.

The dynamic spectra of SSPs were also measured by solar spectropolarimeters in China (National Astronomical Observatory of China (NAOC), Chinese Solar Broadband Radio Spectrometer (SBRS)) [27]. The instruments received dynamic spectra with high time (to 5–6 ms) and spectral (20 MHz) resolution in the frequency band of 5.2–7.6 GHz, including the SSRT reception frequency.

To study the fine temporal structure of X-ray radiation, the instruments CGRO/BATSE [28] (time resolution of 64 ms), RHESSI [29] (100 ms), and FERMI [30] (64 ms) were also used. Also mentioned should be the X-ray spectrometer Konus/Wind [31], in the flare observation mode of which light curves are recorded in three energy channels of 13–50, 50–200, and 200–750 keV with a time resolution of 2–256 ms.

4. Observation data on subsecond pulses

4.1 Dependence of source sizes on the position on the disk

The idea of the compactness of narrowband SSP sources is based on the coherent nature of the generation mechanism. The size of the radiating area L can be estimated as

$$L = \lambda \frac{\Delta f}{f}, \quad (4)$$

where $\Delta f/f$ is the relative radiation bandwidth, and λ is the scale of inhomogeneity of plasma density in the case of plasma radiation or magnetic field inhomogeneity for an ECM. In estimates, the scale $\lambda = 10{,}000$ km is commonly assumed, which is of the order of the typical size of flare magnetic loops. For the characteristic relative width $\Delta f/f = 0.01$, we get for L an estimate of a few hundred kilometers or less than $1''$, which is much smaller than the directional pattern of existing radio heliographs.

However, among the first SSPs recorded at the SSRT, a series of intense subsecond bursts with anomalously large visible sizes (up to $40''$) were recorded during the powerful limb flare on November 2, 1992 [32]. Moreover, the height of the SSP source above the limb appeared unexpectedly large, reaching 35,000 km. The SSP duration did not exceed a few ten milliseconds, and the flux up to 1000 sfu was of the order of the radiation flux of the background solar flare and an order of magnitude higher than the flux from the quiet Sun. The large height of the source contradicted the maser SSP generation model generally accepted at that time [2, 33, 34], since, for ECM generation at the SSRT reception frequency of 5.7 GHz, the magnitude of the magnetic field in the source at a height of 35,000 km had to reach a nonrealistic value of a few hundred gauss.

It became possible to understand the reason for the anomalously large dimensions of the SSP source using the gradually accumulated array of SSP observations at the SSRT. It turned out that the visible size of the sources grows with distance from the center of the Sun disk. Near the disk center, the size is less than $10''$, and in the near-limb regions, it reaches a few ten arc seconds. The experimental dependences of the SSP source sizes on the position on the Sun disk, obtained from data on the 22 and 23 cycles of activity, are shown in Fig. 2 [35, 36]. The SSP database used in the study is available at https://badary.iszf.irk.ru/Ftevents.php.

The growth of the visible size of a near-limb source is explained by an increase in the path length of the electromagnetic radiation in the scattering layer of the solar corona. The dependence obtained at the SSRT is close to the theoretical one presented in Ref. [15]. The detailed analysis of the experimental dependence shown in Fig. 2 was carried out in Ref. [16], where for the first time the plasma density fluctuations in the lower solar corona were estimated: the quadratic fluctuations of the concentration related to hundred meter scales amount to 3–5% of the mean value. It was concluded that in the lower corona the energy spectra of flicker-type plasma turbulence are realized with a spectral index of about 3, for which the energy flux to the small-scale region is absent. Such spectra were observed in the solar wind using radio transmission at distances of several solar radii. Thus, indications have been obtained that the energy spectrum of solar wind fluctuations can be established already in the lower layers of the solar corona.

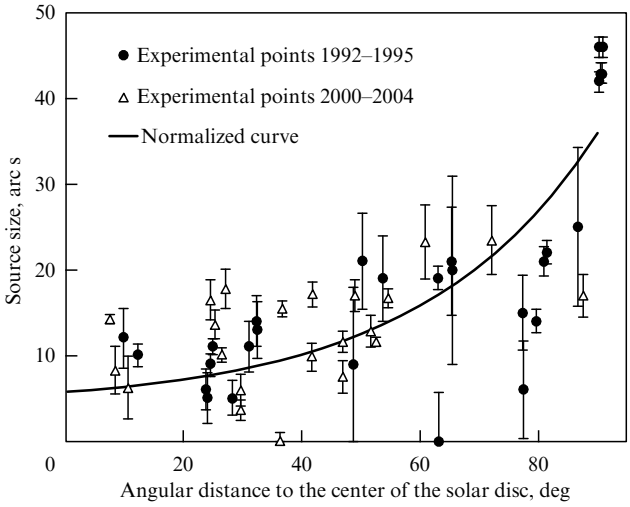

Figure 2. Dependence of the SSP visible size on the angular distance from the center of the Sun disk. Circles show the size of the sources, obtained from observations of 1992–1995, triangles, from observations of 2000–2004. Solid curve corresponds to the Bastian theoretical dependence normalized to experimental data by the least-square method.

The scattering of radiation leads not only to an increase in the visible size but also to the extension of the SSP radiation in time. For limb sources, the spread can reach 50 ms at a frequency of 6 GHz.

The short duration and narrow band of SSPs in combination with the small size of the sources allow considering them a test source for studying the properties of the medium through which its radiation propagates. The visible angular size of point sources changes with the radiation frequency as $\sim 1/f^2$. At the frequency of 17 GHz received by NoRH, the scattering contribution does not exceed a few arc seconds, and the dimensions of the SSP sources were close to the radioheliograph beam [37–39]. In the meter range, the scattering effects substantially affect the characteristics of type II and type III bursts, observed by LOFAR (Low-Frequency Array) in the outer corona of the Sun [40, 41]. Scattering in the interstellar medium substantially affects the properties of radio pulses from pulsars [42–44]. The angular broadening due to scattering imposes substantial limitations on observations of the fine spatial structure in the centimeter range, and its estimations are of great interest for developing projects of new radioheliographs.

4.2 Effects of radiation reflection from the solar atmosphere underlayers

The visible size and shape of an SSP source can be affected by reflection of the SSP radiation from the lower-lying plasma structures, which gives rise to pedestals in the observed brightness distributions. The influence of plasma surrounding the SSP source is especially significant for narrow-band SSPs, whose radiation frequency is close to the plasma frequency or its harmonic. Under these conditions, the propagation of electromagnetic radiation is substantially affected by absorption and refraction. If the source is shielded from above by a plasma layer with a concentration comparable to that in the source, then the flux of its radiation directly towards Earth will be suppressed and it will be possible to observe the reflection of SSP radiation from denser layers of the solar atmosphere located under the SSP source. Such an event was observed on September 17, 2001,

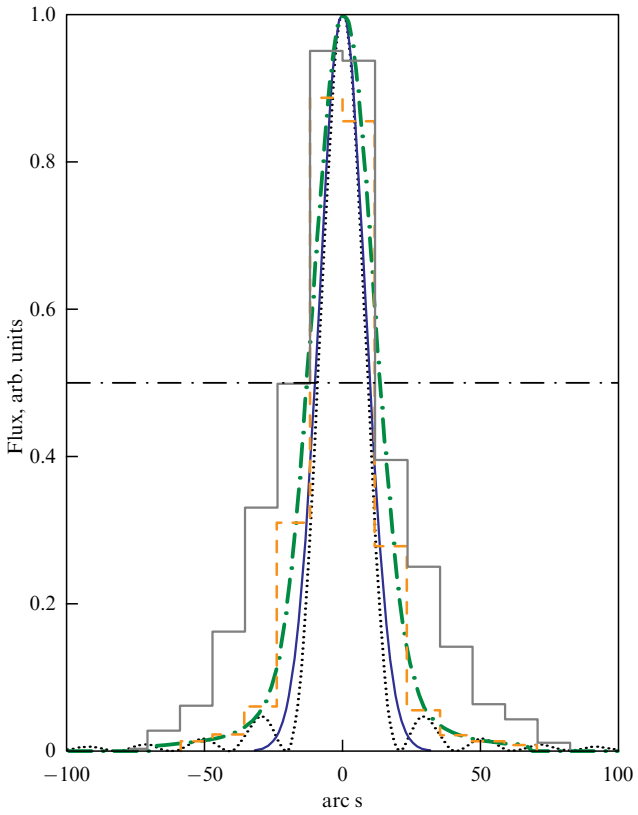

Figure 3. Analysis of the spatial structure of the SSP source recorded by the north–south antenna array. Solid grey stepped line shows the intensity difference scan (R + L); when the background is subtracted from the peak, the measurement step is 10.5″. Black dotted line shows the directional pattern of the north–south antenna array. Solid blue line shows the Gaussian source with a half-maximum width of 20″. Orange shading and the green dashed-dotted line show the result of convolution of the source with the beam with and without the measurement step taken into account on the scale distance–frequency, respectively.

when a flare occurred near the center of the Sun disk (S12E06), where scattering is insignificant, and the visible SSP source had a length of $\sim 15''$ ($\approx 10^9$ km) along the scanning direction [45].

A scan of the SSP source is shown in Fig. 3. Its shape significantly differs from Gaussian. The calculations (dotted and dashed-dotted lines and the histogram) show that the observed shape of the scan can be obtained by a convolution of the SSRT directional pattern with the model point source located at a height of 5500 km above the reflecting surface. In the data from the 23rd cycle, such a pedestal was observed in one third of SSPs.

It should be noted that the influence of the reflection effects on the characteristics of type III bursts in the meter range were discussed earlier in Refs [46, 47] to explain echo-like bursts. The observations of microwave SSPs with spatial resolution confirm the existence of this reflection effect.

4.3 Polarization properties

Reference [48] analyzes the positions of SSP sources, generating at a frequency of 5.7 GHz, relative to the magnetic configuration of the active region. In SSRT observations during the period from 2000 to 2003, about 100 bursts of subsecond duration were recorded, the statistical processing of which showed that the sign of the SSP circular polarization, as a rule, is opposite to the polarization sign of the background flare microwave burst. In this case, the degree of polarization demonstrates no explicit longitude dependence. The origin of the background burst is related to the gyrosynchrotron radiation of non-thermal electrons, its preferable mode of electromagnetic wave in the background bursts being an extraordinary wave. A statistical conclusion that follows is that the mode of the subsecond pulse wave is an ordinary wave. The positions of radio brightness centers for the sources of background bursts and subsecond pulses in most cases do not coincide. In some cases, the difference in positions reaches 1′.

These results were complemented in Ref. [36] using extensive material. It was shown that the SSP sources appeared at latitudes less than 40°. Half of all events have a low degree of polarization (to 5%), mostly having occurred in the central part of the solar disk (longitude interval of 30°E – 30°W) with the polarization sign corresponding to an ordinary wave.

To study the location of sources relative to the magnetic field structure, SSPs with the polarization degree above 30% were chosen, the sources of which were in the central part of the disk, where the projection effects are minimum and no polarization sign inversion because of the quasitransverse propagation of waves on their way from the source should occur. Overlaying SSRT radio maps and longitudinal field magnetograms from the Michelson Doppler Imager (MDI)[2] showed that the SSP sources gravitate towards the line separating the polarity of the vertical magnetic field. This arrangement indicates the location of the sources at the tops of magnetic loops. In SSP bursts from the sources located in the regions of a definite magnetic field sign, i.e., remote from the neutral line by more than 10″, an ordinary mode of electromagnetic radiation is recorded.

Unique data on the source positions of SSPs emitted in one flare at different frequencies could be obtained in combined observations with the SSRT, the 4–8 GHz spectro-polarimeter, and the RATAN-600 (Radioastronomic Telescope of the Academy of Sciences) multiwave radio telescope [49, 50]. For the first time, the positions of a source of microwave type III bursts were determined: at a frequency of 5.7 GHz in both coordinates, and at frequencies of 4.5, 4.7, 4.9, 5.1, 5.3, 5.5, and 6.0 GHz in one coordinate (Fig. 4). The sources were distributed along the direction of emerging magnetic loops, the radiation frequency decreasing towards the loop top [51]. Since type III bursts are emitted through the plasma mechanism, the radiation frequency of which is proportional to the root of the local plasma concentration, these results allowed determining the concentration change along the loop and showed the prospective potential of using multifrequency observation of short pulses to measure the parameters of plasma in flare loops.

4.4 Spectral characteristics of subsecond pulses

The Huairow and the BBMS dynamic spectra recording the integral solar radiation in the range of around 5.7 GHz, the SSRT reception frequency, showed that the spectra of subsecond pulses can significantly differ and, therefore, the SSPs can be generated by different mechanisms. The main structures are broadband pulsations, spikes, i.e., narrow-

[2] MDI (Michelson Doppler Imager) [52] is an instrument aboard the SOHO (Solar and Heliospheric Observatory) satellite to measure magnetograms of the total solar disk with a spatial resolution of 1.98″ and time resolution of 96 min.

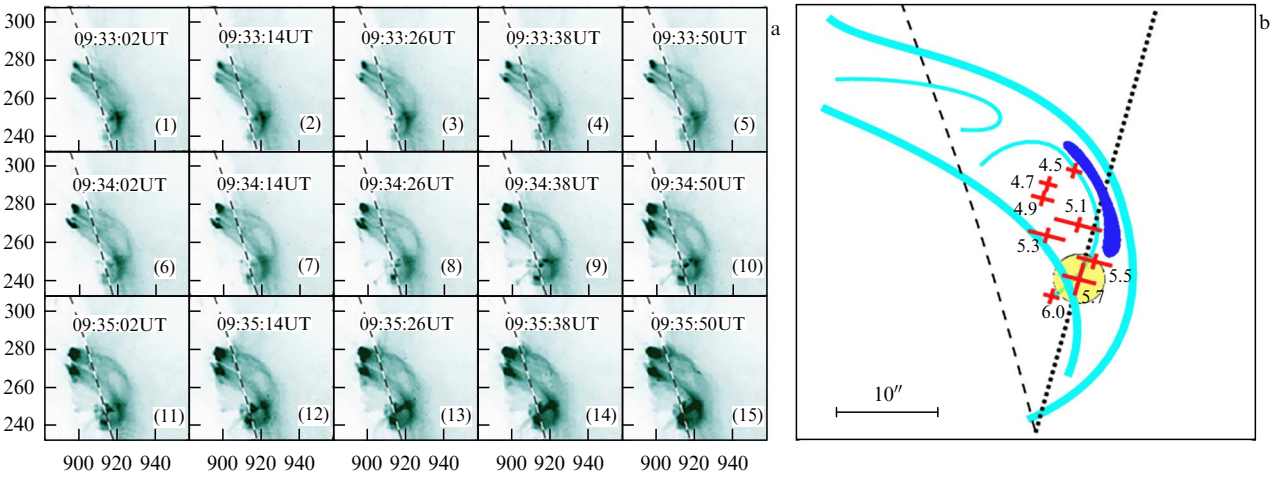

Figure 4. Development of the active region during the flare of August 10, 2011 in extreme ultraviolet radiation of 94 Å according to data from AIA/SDO (Atmospheric Imaging Assembly/Solar Dynamical Observatory[3]) (a) and schematic illustration of the localization of microwave sources of bursts (b). Position of the source at 5.7 GHz is shown with a yellow dot (b). Drifting extended source seen in the series of UV shots is shown blue. Dotted line in Fig. b is the direction of the axis of the knife-edge directional pattern of RATAN-600. Sizes of microwave sources shown by bars with the frequency indicated. Slanted dashed line (a, b) marks the Sun limb.

band bursts without frequency drift, and bursts with frequency drift, like type III bursts in the meter and decimeter range [1]. In the centimeter range, the measurements of spectral bandwidth were first performed for narrow-band driftless subsecond pulses, known as spikes [54]. It was shown that the relative width of the spectrum could be less than one percent and change a fewfold during one flare event.

4.4.1 Broadband subsecond pulses and electron acceleration mechanisms. Reference [55] describes observations of short pulses at a frequency of 17 GHz, which were interpreted as gyrosynchrotron radiation from pulsed flows of accelerated electrons precipitating into the lower layers of the solar atmosphere. In SSP observations at frequencies of 5.7 and 17 GHz, this conclusion was confirmed and the energy of electrons precipitating into the base of flare loops was determined to be 100–200 keV [39]. When these electrons decelerate in a dense plasma of the bases, pulses of hard X-ray radiation are recorded.

The duration of short broadband pulses is comparable to the subsecond times of flight of the accelerated electrons along the flare magnetic loops, which allows measuring the dependence of their relative delays on the energy of electrons emitting in the microwave and hard X-ray ranges. In combination with knowledge about the radiation source location, these dependences offer unique information about the place and characteristics of the acceleration region in a solar flare. A striking example of the analysis of a broadband SSP observation is the SOL2011-08-04 flare [56]. Figures 5 and 6 show temporal profiles of the flare radiation with broadband pulses in the hard X-ray and microwave ranges.

Analyses of SSP characteristics have shown that nonthermal electrons are energy distributed according to a power law and propagate along the magnetic field in a narrow cone. The electrons are accelerated during the pulse with a duration of less than 50 ms in a compact region near the top of a flare loop. Overall, the observation data testify to the acceleration of electrons to an energy of 1–2 MeV in super-Dreicer electric fields, regular or stochastic. These results on the character of the primary release of energy in a solar flare, based on the observation of broadband SSPs, were obtained in Ref. [57].

4.4.2 Narrow-band bursts. In cases when structures with a narrow instantaneous spectral band (e.g., spikes and drifting bursts) are observed in the dynamic spectra, the SSP emission is interpreted within the framework of coherent radiation mechanisms. The electron cyclotron maser mechanism was proposed to interpret the first observations of decimeter and meter SSPs [2, 34, 58]. However, it turns out that the requirements for the relation between plasma density and the magnetic field magnitude, $f_{pe} \leqslant f_{ce}$, the angular distribution of nonthermal electrons, and the conditions for radiation exit impose serious limitations on the possibility of implementing the ECM mechanism in the solar atmosphere. To date, there is still no convincing experimental evidence of the realization of this mechanism in the atmosphere of the Sun.

In events for which estimates of the concentration and magnetic field in SSP sources were possible, the ratio of frequencies was reciprocal: $f_{pe} \gg f_{ce}$. As a rule, SSP sources are located far from strong magnetic fields, often near the neutral lines separating vertical magnetic field components of opposite signs, where the frequency of the SSP radiation corresponds to the 5–10th harmonic of the cyclotron frequency, at which the maser mechanism is not efficient [2, 13].

On the other hand, the hypothesis of the plasma mechanism of SSP emission agrees with the observed, preferably low degrees of polarization with the O-mode sign. The difficulties in the plasma interpretation arise when determining the mechanism of conversion of plasma oscillations into electromagnetic waves and providing the conditions for the radiation's exit into the outer corona. Note that, to generate SSPs at the fundamental SSRT reception frequency (5.7 GHz), the concentration of plasma in the

[3] The Atmospheric Imaging Assembly (AIA) instrument aboard the Solar Dynamics Observatory (SDO) space station, recording the ultraviolet radiation of the entire solar disk with spatial ($\sim 1.5''$) and temporal (12 s) resolution in seven channels, corresponding to the lines of ionized iron: Fe XVIII (94 Å), Fe VIII, XX, XXIII (131 Å) , Fe IX (171 Å), Fe XII, XXIV (193 Å), Fe XIV (211 Å), He II (304 Å), Fe XVI (335 Å). The AIA also records radiation in the line C IV (1600 Å) and the continuum (1700, 4500 Å), corresponding to the photosphere and transition layer [53].

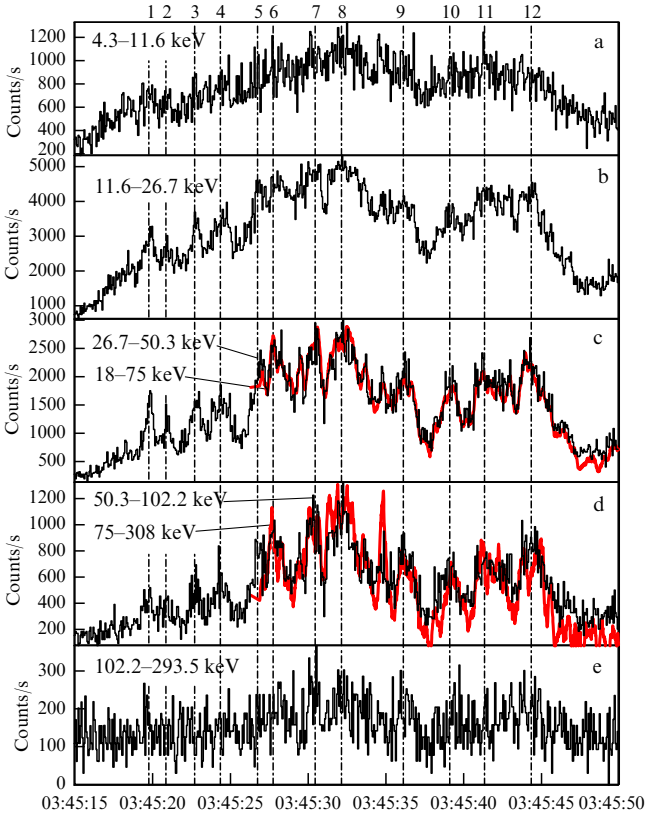

Figure 5. Flare of August 4, 2011. Intensity of hard X-ray radiation in channels of Fermi Gamma-ray Space Telescope/Gamma-ray Bust Monitor (FERMI/GBM) (black curves) and Konus-Wind 18–75 and 75–308 keV (red curves). Vertical dashed-dotted lines mark moments of time when SSPs were observed.

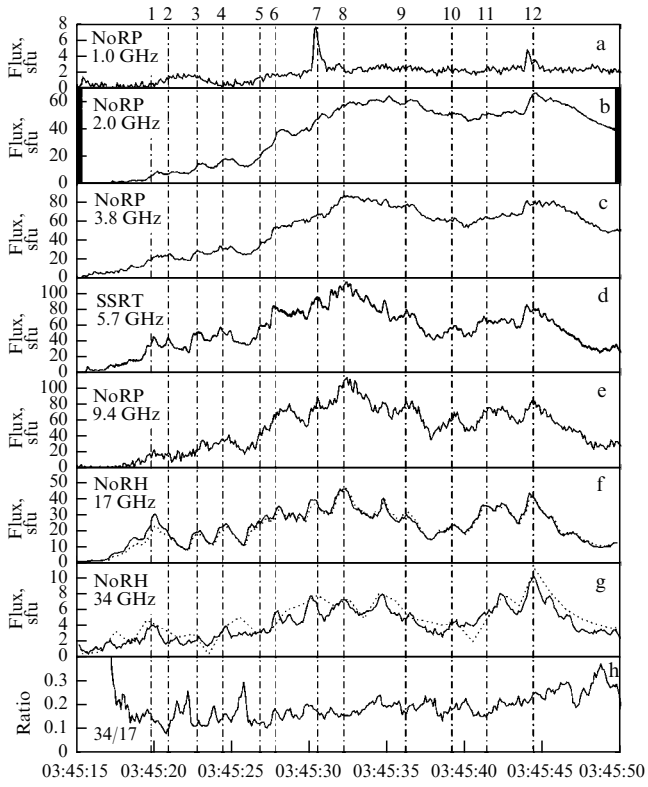

Figure 6. Flare of August 4, 2011. Microwave profiles measured with the NoRP and NoRH instruments at various frequencies. (f, g) Solid lines show correlation curves, dotted lines show fluxes obtained from NoRH images at 17 and 34 GHz, respectively; (h) ratio of signals at 34 and 17 GHz. Vertical dashed-dotted lines mark moments of time at which SSPs were observed.

source should be relatively high, 4×10^{11} cm^{-3} for coronal flare structures. The requirement for the plasma density is softened to 10^{11} cm^{-3} if the SSP electromagnetic radiation is generated at a frequency close to the doubled plasma frequency. Note that the high concentration of plasma in the source, as opposed to the environment, facilitates the exit of radiation to the outer corona [14].

A coherent mechanism of emission can provide such high SSP radiation power that, even after a decrease in the radiation by orders of magnitude while passing a few absorption lengths, the SSP can be detected on Earth. In this case, the emergent SSP radiation will be collimated and can change the polarization sign to the extraordinary mode due to different absorption coefficients for ordinary and extraordinary waves.

4.4.3 Bursts with frequency drift — an analog of type III meter bursts. Frequency-drifting microwave narrow-band structures were discussed in Refs [59–64]. The change in the radiation frequency is explained by the motion of a beam of emitting electrons across the gradient of plasma concentration, due to which the plasma frequency, proportional to the square root of the plasma concentration, changes in the generation region. It was found that, in contrast to the meter range, where the drifts are directed towards lower frequencies, in the centimeter range, opposite drifts, i.e., towards higher frequencies, are often observed. The opposite drifts are observed while the beam moves down along the loop into the denser plasma. In addition, in microwaves, the range of absolute values of frequency drift rates is much wider, 0–20 GHz s^{-1}. Low drift rates are observed during intervals of time when the radiation sources (electron beams) move near the top of the flare loop, where the density variation along the motion path is small.

A new stage in studies of drifting bursts in the centimeter range has begun with interferometric observations, which allowed localizing their sources in flare loops. Analysis of the large array of bursts simultaneously recorded in 2000–2004 by the SBRS spectropolarimeter in Huairow (Beijing) (5.2–7.6 GHz) and the SSRT (5.7 GHz) has shown [18, 65–67] that the drifting bursts are radiated at a harmonic of the plasma frequency, and the drift rates in most bursts (72%) fall within 3–13 GHz s^{-1} and are distributed around a mean value of about 7 GHz s^{-1}.

An example of the dynamic spectrum is shown in Fig. 7. In the present case, the frequency drift was opposite with a rate of 8.5 GHz s^{-1}, the SSP source being simultaneously observed in two interference orders of the SSRT at frequencies of 5.69 and 5.78 GHz [68]. Simultaneous observations in two orders make it possible to determine the difference among the source positions at these frequencies, i.e., to measure directly the plasma concentration gradient along the exciter motion path. Figure 7c shows the displacements of the SSP brightness centroids with respect to the centroid of the background burst. It is seen that the difference among SSP source positions observed at these two frequencies reaches $\Delta l \approx 3''$.

Events in which tens of SSPs are recorded during a limited interval of time turned to be of most interest. Figure 8

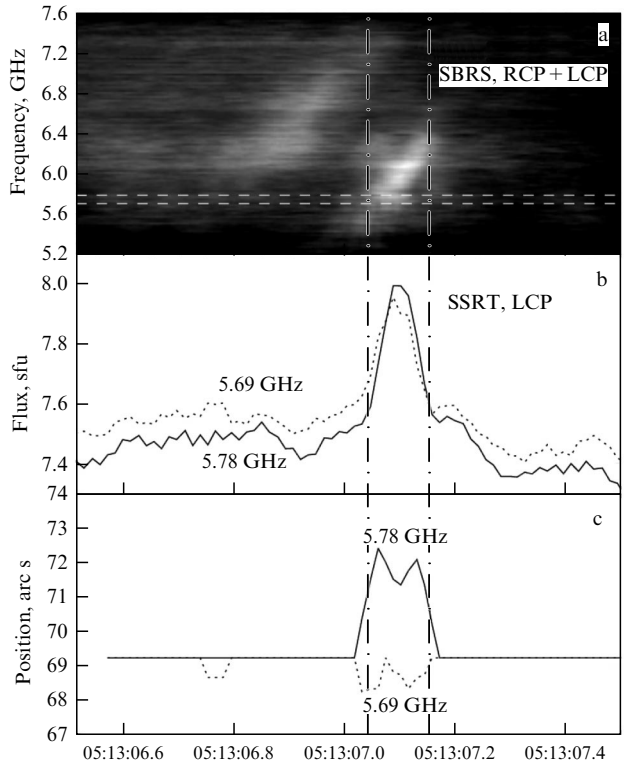

Figure 7. March 30, 2001. Subsecond pulse, recorded at two SSRT frequencies. (a) Dynamic spectrum (intensity, NAOC). Horizontal dashed lines mark the SSRT reception band. (b) Time profiles at 5.69 GHz (dotted curve) and 5.78 GHz (solid curve). (c) Time variation of centroid positions of sources of SSPs at two frequencies. Vertical dashed-dotted lines mark the interval of time when the rapidly drifting component in the spectrum was observed.

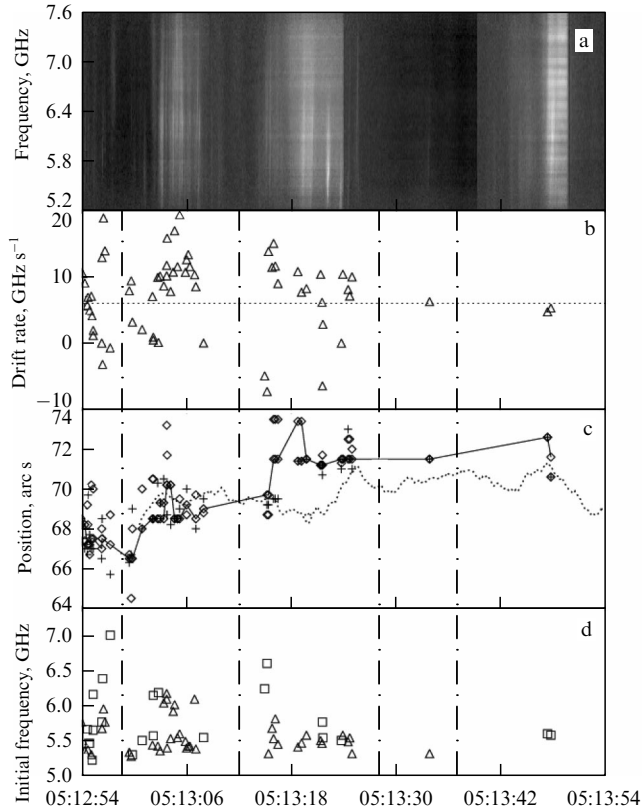

Figure 8. Characteristics of subsecond pulses: (a) NAOC dynamic spectrum; (b) drift rates obtained from the NAOC data: dotted horizontal line marks the mean drift rate of 6 GHz s^{-1}; (c) SSP source positions on SSRT one-dimensional brightness distributions (scans); diamonds — at a frequency of 5.78 GHz, crosses — at 5.69 GHz, solid line shows 'centers of gravity' of background burst scans; (d) initial frequency. Vertical dashed-dotted lines mark time intervals with individual series of SSPs.

presents the dynamic spectra and kinematic characteristics of 67 bursts recorded in 1 min, whose sources were located in the flare loop, elongated in the direction of scanning. Figure 8b shows that, as a rule, the drift occurs towards higher frequencies, and the rates are distributed symmetrically with respect to the value of 6 GHz s^{-1}.

Changes in the location of the sources at frequencies of 5.69 and 6.78 GHz (Fig. 8c) gradually shifting to the north do not correlate with the values of the drift rate. The difference Δl in many cases is insignificant. For example, in the last SSPs, $\Delta l \approx 0$, the drift rate being about 6 GHz s^{-1}.

To measure the exciter velocity, we use an expression for the frequency drift rate, in which, instead of the commonly used partial derivative, a total time derivative of the plasma density is used:

$$\frac{\mathrm{d}f}{\mathrm{d}t} = \frac{A}{2\sqrt{n}}\frac{\mathrm{d}n}{\mathrm{d}t} = \frac{A}{2\sqrt{n}}\left(\frac{\partial n}{\partial t} + \frac{\partial n}{\partial x}\frac{\partial x}{\partial t}\right)$$

$$= \frac{A}{2\sqrt{n}}\left(\frac{\partial n}{\partial t} + \frac{\partial n}{\partial x}v\right) \approx 2\Delta f\left(\frac{1}{\tau_{\mathrm{SSP}}} - \frac{v}{\Delta l}\right), \qquad (5)$$

where $A = (1/\pi)\sqrt{4\pi e^2/m}$. The measured quantities are the drift rate $\mathrm{d}f/\mathrm{d}t$, the difference among observation frequencies $\Delta f = 0.09$ GHz, and the displacements of centroids Δl. To calculate the velocity v, it is necessary to estimate the term $1/\tau_{\mathrm{SSP}}$, which describes the plasma density change in the source with time and usually is not taken into account in the analysis of type III bursts. In our case, the calculation of the exciter velocity without this term for some SSPs leads to an overestimation of the exciter velocity up to twice the speed of light. Cases with zero displacement yield an estimate of the reciprocal rate of concentration increment in the SSP sources $\Delta f/\tau_{\mathrm{SSP}} \approx 6$ GHz s^{-1}. This suggestion is confirmed by the symmetry of the distribution of frequency drift rates with respect to this value.

Figure 9a shows the dependence of the source motion velocity on the value of displacement Δl. The velocities of the emitting agent vary in wide limits from -1.6×10^{10} to 2.9×10^{10} cm s^{-1}. From a histogram of the exciter velocities (Fig. 8b), it follows that in most SSPs the absolute values of exciter velocity are less than 5.0×10^9 cm s^{-1}, which is an order of magnitude smaller than the usual velocity of electrons obtained for meter and decimeter type III bursts. The relaxation time for electrons with such a velocity due to Coulomb collisions in the plasma with a density of 10^{11} cm^{-3} does not exceed 0.04 s and is much smaller than the SSP duration in Fig. 9c [66]. The resolution of the controversy consists in the assumption that at low exciter velocities the burst is generated by fast electrons with larger pitch angles and, therefore, a small velocity component along the flare loop. It is reasonable to assume that each SSP corresponds to a pulse of acceleration of electrons with the increment of plasma density in the current layer [69]. Then, from the estimate $\Delta f/\tau_{\mathrm{SSP}} = 6$ GHz s^{-1}, it follows that the plasma concentration growth rate in the region of SSP generation is 1.25×10^{11} cm^{-3} s^{-1}.

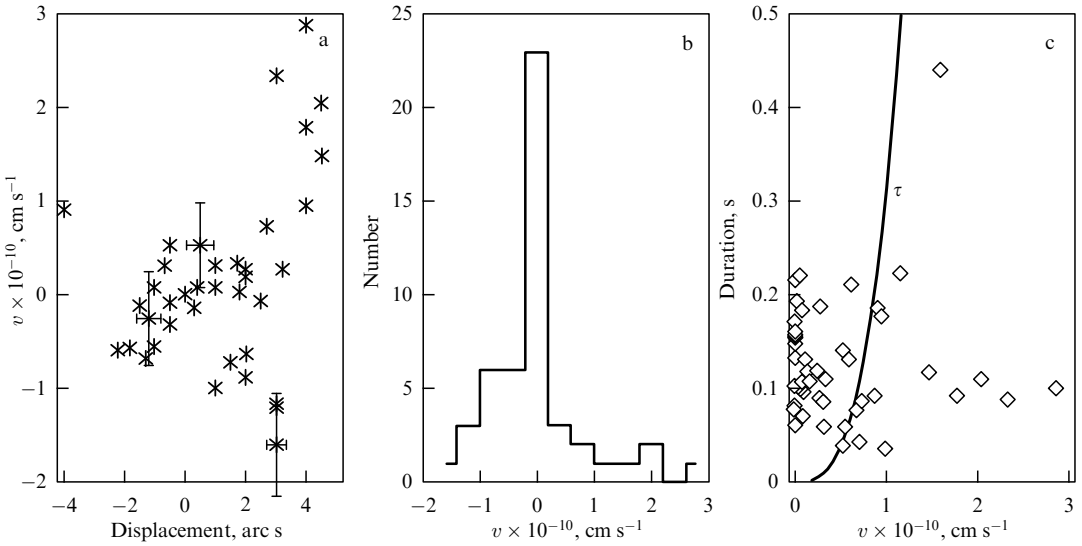

Figure 9. March 30, 2001. (a) Dependence of source velocity v on displacement Δl; positive values correspond to displacements to the north. For three cases, errors in determining the parameters (three root mean square deviations) are shown. (b) Histogram of exciter velocities. (c) Relation between absolute values of the source velocity and burst durations. Solid curve shows the relaxation time of electrons depending on their velocity.

This result on the distribution of SSPs over the frequency drift rates was confirmed in Ref. [70], in which a series of 56 bursts recorded for 30 s was discussed. In this case, the mean rate of frequency drift was equal to 3.6 GHz s^{-1}.

Usually, observations of type III bursts are considered a direct response to beam instability, excited by electron beams propagating along magnetic field force lines. In the microwave range, the discovery of a large pitch angle anisotropy of radiating electrons and a small velocity of the source motion along the flare loops evidence in favor of cone instabilities which can excite upper-hybrid plasma waves [2, 71, 72]. Electromagnetic radiation at the double plasma frequency is generated at a nonlinear coupling of upper-hybrid waves.

4.4.4 U-type bursts. When electron beams move along closed magnetic loops, the appearance of bursts of the inverse J and U type in the dynamic spectra is possible, whose shape reflects the motion of the emitting beam from the footpoint of the loop, where the plasma density is minimum, to the top. Such structures are often observed in the dynamic spectra in the meter and decimeter ranges [73–76].

Figure 10a displays the dynamic spectrum of a burst during the flare of September 17, 2001. If different branches of the burst correspond to different footpoints of the flare loop, then the difference in the positions on the Sun disk would be sufficient for resolving them in space in SSRT scans. However, it turns out that the position of the radiation source remains practically unchanged during a U-burst (Fig. 10d, e). In the archive of joint observations of the SSRT and the NAOC spectropolarimeters, four events with U-bursts could be found [65]. All events were short-term, and the delay between the moments of recording the ascending and descending branches did not exceed 0.5 s in any of the events found. No displacement of sources during the U-bursts was observed either. Therefore, the changes in the spectrum of the microwave U-burst are not related to the beam of electrons moving from one footpoint of a loop to another.

In Ref. [65], a new scenario for generating such microwave bursts was proposed, schematically shown in Fig. 11. In this scheme, U-structures in the dynamic spectra appear when a

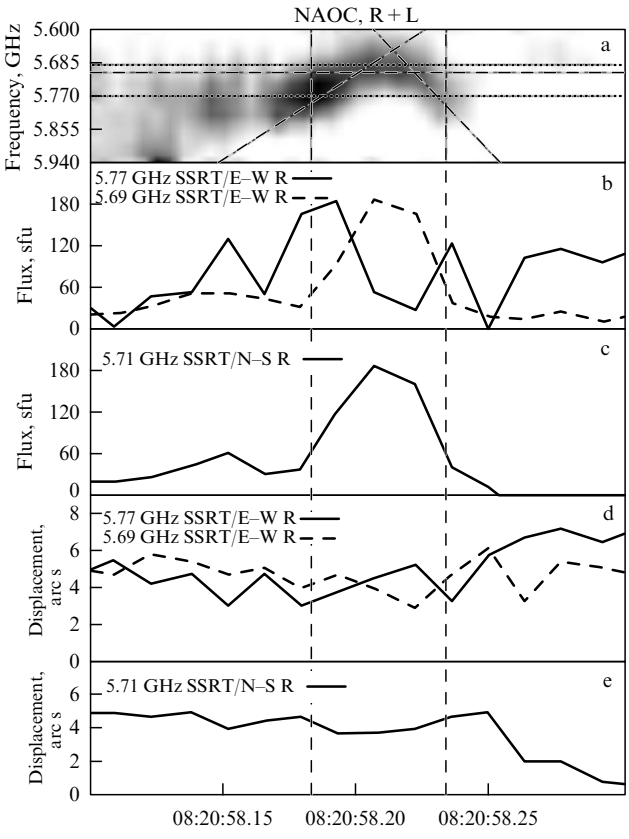

Figure 10. September 17, 2001. Spectral and temporal characteristics of a U-burst. (a) Dynamic spectrum. Horizontal lines show the frequencies of registration by antenna 1D arrays N–S (dashed line) and E–W (double dotted line). (b, c) Time profiles at SSRT reception frequencies. (d, e) Spatial displacements of brightness centroids. Vertical lines mark ends of U-burst branches.

beam of emitting electrons passes a segment of the magnetic loop in which magnetohydrodynamic 'sausage' oscillation are excited, leading to plasma density modulation and, therefore, to the modulation of the radiation frequency.

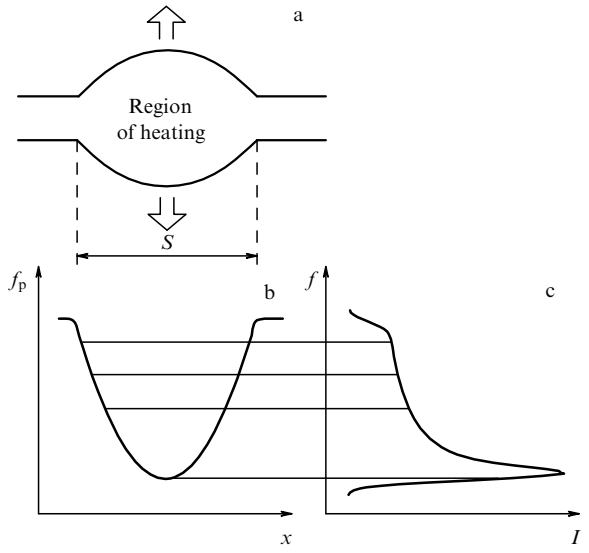

Figure 11. (a) Schematic of U-burst generation; S is the size of the region emitting radiation. (b) Instantaneous profile of brightness; x is distance, f_p is plasma frequency. (c) Spectrum of radiation response; I is intensity, f is frequency.

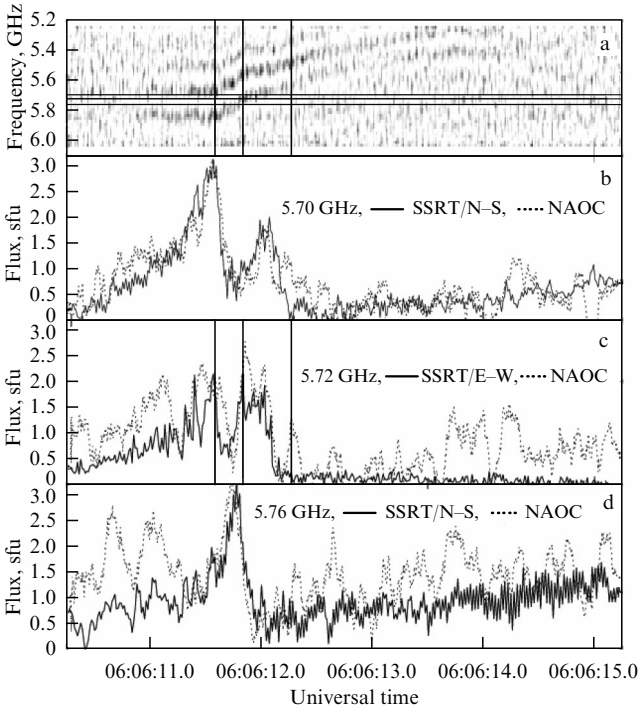

Figure 12. Flare of January 5, 2003 with a zebra pattern. (a) NAOC dynamic spectrum. Horizontal lines show SSRT reception frequencies. (b–d) Time profiles recorded by NAOC spectropolarimeters and SSRT antenna arrays at close frequencies.

Small-scale plasma oscillations can be excited in this region by the cone instability of the captured electrons.

The processes of pulsed energy release can excite MHD oscillations. Observations of hard X-ray radiation pulses with a duration of about 10 ms are known [77]. The existence of local heating regions in flare loops is confirmed by observations in soft X-ray and extreme ultraviolet radiation [78–81].

The instantaneous spectrum and spectral width of plasma radiation are determined by the distribution of density in the radiating region. Figure 11b implies that the plasma density is distributed according to a parabolic law. At each moment of time, the maximum of the radiation spectrum (Fig. 11c) corresponds to the plasma density in the middle of a hot region, where the concentration gradient is minimum.

Thus, in the dynamics of microwave radiation, a response to the pulsed heating of a limited part of the magnetic loop is observed. Radiation at frequencies close to local Langmuir ones is generated as a result of exciting the plasma turbulence by electron beams propagating along a magnetic loop and the subsequent conversion of longitudinal plasma oscillations into electromagnetic radiation. The instantaneous width of the emission band is determined by the shape of the plasma density distribution in the emitting region.

4.4.5 Zebra bursts. A zebra pattern is observed in the dynamic spectra as a set of practically parallel bright and dark stripes. Measurements of the distances between the stripes can be used to diagnose the magnetic field in the coronal regions. To date, a few mechanisms for generating this type of radiation have been proposed, which can be divided into two groups [82]. In the first one, it is assumed that all stripes are generated in one source at harmonics of a natural frequency, e.g., the cyclotron frequency [83–85]. In the second group of models, individual stripes are generated at different sites, where certain resonance conditions are fulfilled. In these cases, the separation between the stripes can change over the spectrum and depends on the type of wave excited in the emitting structure [86–91].

Note that observations of microwave zebra patterns with radioheliographs, which could allow determining the radiation source in the flare and assess the plasma parameters independently, are extremely few. Figure 12 shows the zebra pattern with several equidistant stripes in the range of 5–6 GHz [91]. SSRT observations showed that the visible size of the source does not exceed 10″, and the positions of the sources of different stripes of the zebra pattern coincide. The degree of circular polarization of the radiation reaches 100%, and the sign of the polarization corresponds to an extraordinary wave (X-mode). The high degree of polarization, its sign (extraordinary wave), and the equidistant arrangement of the spectrum stripes allowed identifying the generation mechanism as the nonlinear merging of harmonics of Bernstein modes, excited at the frequencies of cyclotron oscillations of electrons [92]. The process of nonlinear merging converts the electrostatic oscillations of modes into electromagnetic radiation in the frequency range from the fundamental plasma frequency to its harmonic. The radiation frequency indicates a plasma density in the source of $\sim 10^{11}$ cm^{-3}, and a frequency interval of 0.16 GHz between adjacent stripes corresponds to the electron cyclotron frequency at a magnetic field strength of 60–80 G. These estimates agree with magnetic field calculations and the value of plasma density obtained from observations in extreme ultraviolet radiation.

Several events with zebra patterns, in which the condition of equidistant stripes was not fulfilled, are described in Refs [93, 94]. The sources of zebra patterns were located in the coronal part of flare loops, in which the magnetic field was about a few hundred gauss. The radiation frequencies of zebra patterns of ~ 6 GHz were close to the local doubled Langmuir frequency at 10^{11} cm^{-3}. The frequency jumps between the stripes were within the limits of 0.1–

0.7 GHz. To interpret the observations, two mechanisms were used.

In the first, the zebra pattern was generated during the excitation of cone instability by electron fluxes with large pitch angles [95]. Bright *s*-stripes in the dynamic spectra are generated at frequencies f^s at sites on a flare loop, where the conditions of double plasma resonance are fulfilled:

$$f^s = \sqrt{f_{\rm p}^2(n^s) + f_B^2(B^s)} = s f_B(B^s)\,. \qquad (6)$$

Here, $f_{\rm p}$ is the frequency of the plasma wave at plasma density n^s at the site of *s*-strip generation, and f_B is the cyclotron frequency in the magnetic field B^s. The conditions of resonance in the recorded zebra patterns can be fulfilled for the resonant harmonics $s = 2-8$. Then, in the merging process, the excited higher-hybrid waves generate electromagnetic radiation at frequencies close to the doubled local Langmuir frequency.

The second mechanism is based on the interaction of plasma waves with whistler waves excited by electrons with a cone angular distribution [3, 94]. In this case, the frequency jump must be about the whistler frequency, which was within $(0.1-0.25) f_{\rm pe}$.

Among 200 events with a fine temporal structure recorded by Chinese spectropolarimeters together with the SSRT in the frequency range from 5.2 to 7.5 GHz, there were six events of the 'zebra' type. Their intensity did not exceed a few solar flux units. It can be expected that high-sensitivity multiwave radioheliographs of the new generation will allow identifying the generation mechanism and realizing the high diagnostic potential of the observation of zebra patterns.

5. Discussion of results and prospects of studies of microwave subsecond pulses

One of the main characteristics of energy release in various astrophysical objects is the generation of accelerated nonthermal particles. Subsecond pulses of radio emission are an important source of knowledge about the processes of acceleration *in situ*, as well as about the properties of a medium on the path of wave propagation to the observer. Along with the magnetosphere of Earth, the Sun is the nearest space observatory, which makes it possible, if not to resolve the structure of the region of electron acceleration to relativistic energies, then at least to localize them on the solar disk, so that it would be possible to determine the main parameters of the plasma at the site of acceleration.

The main physical properties of microwave SSPs are a small duration, a high brightness temperature, their location in a very dense plasma, of the order of 10^{11} cm^{-3}, at least an order of magnitude higher than the background one, the appearance, as a rule, of a flare in the initial or impulsive stage, great variability in the polarization degree from 0 to 100%, and a variety of spectrum forms from narrow-band to broad-band, which indicates different mechanisms of formation.

Even limited information on the dependence of the visible size of SSP sources on their position on the solar disk allowed estimating the parameters of turbulent fluctuations of plasma density in the lower corona. The most important result of SSP observations is the conclusion about the dominance of the plasma mechanism of generating narrow-band radio bursts rather than the cyclotron maser mechanism in the solar atmosphere. It is worth noting that the plasma mechanism is discussed in the interpretation of radiation of brown dwarfs [95]. A close analogy is noticed between solar zebra patterns and the quasiharmonic spectra of microwave radiation of the pulsar in the Crab Nebula [96, 97].

Observations with spatial resolution have shown that, in spite of the morphological similarity between microwave SSPs with frequency drift and type III meter bursts, the characteristics of the angular distribution of the emitting electrons are essentially different. The microwave bursts are generated mainly by fluxes with large pitch angles, which indicates that the acceleration occurs mainly across the magnetic field. It is found that in the microwave range in the analysis of drift rates it is necessary to take into account the increment in the plasma density in the source, which is caused by the inflow of plasma to the reconnection region. Plasma density variations like the 'sausage' mode can manifest themselves as inverse U-like patterns.

Broadband SSPs are evidence of fragmented energy release in solar flares, and analyses of time-of-flight relations in combination with the observation of the position and structure of the sources allow determining the site of primary energy release and the characteristic spatial and temporal scales of the electron acceleration processes.

In many cases, the observed angular sizes of the SSP sources are determined not by their internal structure but by the effects of scattering of electromagnetic waves by inhomogeneities of plasma concentration in the lower solar corona. The measured dependences of the scattering angles made it possible to extend estimates of the spectrum of density fluctuations from the outer corona, where measurements by radio transmission methods are possible, to the lower part of the solar corona. The spectral measurements will be substantially developed with the beginning of observations using multiwave radioheliographs, since the effective cross section of scattering varies quadratically with the change in the observation frequency.

To date, at the Radio Astronomical Observatory of the Institute of Solar-Terrestrial Physics, Siberian Branch of the Russian Academy of Sciences, a large archive of observation results has been collected; a database for 2000–2013 on radio bursts with fine structure is made available via the Internet at https://badary.iszf.irk.ru/Ftevents.php, supplemented by BBMS dynamic spectra (4–8 GHz).

As follows from the above results, the observations of microwave radiation subsecond pulses with spatial resolution provide us with unique information on the nature of flare energy release, the configuration of dynamic structures, and the properties of plasma in the transition region and lower corona of the Sun.

Up-to-date instruments, now under development and testing, will make it possible to realize the diagnostic potential of SSPs due to fast space-resolved observations in a wide range of frequencies. In the microwave range, the largest instruments under construction are the Russian Siberian radioheliograph (SRH, 3–24 GHz) [98, 99], the American Frequency Agile Solar Radiotelescope (FASR) [100], and the Chinese Mingantu Ultrawide Spectral Radioheliograph (MUSER) [101]. To develop and test the systems of the FASR radioheliograph, the Expanded Owens Valley Solar Array (range of 1–18 GHz) is used [102]. The antenna systems CSRH-I (40 antennas, 0.4–2.0 GHz) and CSRH-II (60 antennas, 2–15 GHz) are mounted at the Chinese Mingantu radioheliograph. At present, test observations have started at the SRH in some ranges. The construction of

the Siberian Radioheliograph and the Spectropolarimeters of Integral Solar Radiation (50 MHz–24 GHz) with a minimum time resolution to 0.1 s is planned to be finished in the nearest years [99].

The authors thank the anonymous referees for their useful remarks, which improved the paper. The work was carried out under financial support from the Ministry of Science and Higher Education of Russia. The results were obtained using the unique research facility, the Siberian Solar Radiotelescope, http://ckp-rf.ru/usu/73606. The authors thank V V Grechnev, R A Sych, G P Chernov, V F Mel'nikov, and L K Kashapova for the fruitful discussions.

References

1. Benz A O *Sol. Phys.* **104** 99 (1986)
2. Fleishman G D, Mel'nikov V F *Phys. Usp.* **41** 1157 (1998); *Usp. Fiz. Nauk* **168** 1265 (1998)
3. Chernov G P *Fine Structure of Solar Radio Bursts* (Astrophysics and Space Science Library, Vol. 375) (Berlin: Springer, 2011)
4. Casillas-Pérez G A et al. *Sol. Phys.* **294** 10 (2019)
5. Spitler L G et al. *Astrophys. J.* **790** 101 (2014)
6. Zhdanov D A, Zandanov V G *Central Eur. Astrophys. Bull.* **35** 223 (2011)
7. Gary D E, Hurford G J, Flees D J *Astrophys. J.* **369** 255 (1991)
8. Bregman I D, Netherlands Foundation for Radioastronomy Report No. 330 (1980)
9. Kai K, Nakajima H, in *Rapid Fluctuations in Solar Flares* (NASA. Goddard Space Flight Center, CP-2449, Eds B R Dennis, A L Kiplinger, L E Orwig) (Washington: NASA Conf. Publ., 1986) p. 147
10. Kattenberg A, Allaart M *Astrophys. J.* **265** 535 (1983)
11. Ramaty R *Astrophys. J.* **158** 753 (1969)
12. Zheleznyakov V V *Radio Emission of the Sun and Planets* (Oxford: Pergamon Press, 1969); Translated from Russian: *Radioizluchenie Solntsa i Planet* (Moscow: Nauka, 1964)
13. Melrose D B *Rev. Mod. Plasma Phys.* **1** 5 (2017)
14. Benz A O et al. *Sol. Phys.* **141** 335 (1992)
15. Bastian T S *Astrophys. J.* **439** 494 (1995)
16. Chashei I V, Shishov V I, Altyntsev A T *Astron. Rep.* **50** 249 (2006); *Astron. Zh.* **83** 282 (2006)
17. Grechnev et al. *Sol. Phys.* **216** 239 (2003)
18. Meshalkina N S et al. *Sol. Phys.* **221** 85 (2004)
19. Altyntsev A T et al. *Space Sci. Rev.* **68** 251 (1994)
20. Altyntsev A T et al. *Astron. Astrophys.* **287** 256 (1994)
21. Altyntsev A T et al. *Astron. Astrophys.* **303** 249 (1995)
22. Altyntsev A T et al. *Sol. Phys.* **168** 145 (1996)
23. Nakajima H *Proc. IEEE* **82** 705 (1994)
24. Torii C et al. *Proc. Research Institute of Atmospherics, Nagoya Univ.* **26** 129 (1979)
25. Shibasaki K, Ishiguro M, Enome S *Proc. Research Institute of Atmospherics, Nagoya Univ.* **26** 117 (1979)
26. Nakajima et al. *Astron. Soc. Jpn. Publ.* **37** (1) 163 (1985)
27. Ji H et al. *Sol. Phys.* **213** 359 (2003)
28. Varendorff M *SIF Conf. Proc.* **47** 183 (1995)
29. Lin R P et al. *Sol. Phys.* **210** 3 (2002)
30. Meegan C et al. *Astrophys. J.* **702** 791 (2009)
31. Aptekar R L et al. *Space Sci. Rev.* **71** 265 (1995)
32. Altyntsev A T et al. *Astron. Astrophys. Suppl. Ser.* **113** 415 (1999)
33. Melrose D B, Dulk G A *Astrophys. J.* **259** 844 (1982)
34. Vlasov V G, Kuznetsov A A, Altyntsev A T *Astron. Astrophys.* **382** 1061 (2002)
35. Altyntsev A T et al. *Astrophys. J.* **469** 976 (1996)
36. Meshalkina N S et al. *Adv. Space Res.* **35** 1785 (2005)
37. Shibasaki K et al. *Space Sci. Rev.* **68** 217 (1994)
38. Takano T, in *Proc. of the Eighth Intern. Symp. on Solar Terrestrial Physics, Sendai, Japan, 1994, SCOSTEP*, p. 44
39. Altyntsev A T et al. *Sol. Phys.* **195** 401 (2000)
40. Chrysaphi N et al. *Astrophys. J.* **868** 79 (2018)
41. Gordovskyy M et al. *Astrophys. J.* **873** 48 (2019)
42. Bilous A V et al. *Astron. Astrophys.* **591** A134 (2016)
43. Donner J Y et al. *Astron. Astrophys.* **624** 11 (2018)
44. Kondratiev V I et al. *Astron. Astrophys.* **585** A128 (2016)
45. Altyntsev A T et al. *Astron. Astrophys.* **400** 337 (2003)
46. Wild J P, Smerd S F *Annu. Rev. Astron. Astrophys.* **10** 159 (1972)
47. Abranin E P, Bazelyan L L, Tsybko Ya G *Astron. Rep.* **40** 853 (1996); *Astron. Zh.* **73** 939 (1996)
48. Lesovoi S V, Kardapolova N N *Sol. Phys.* **216** 225 (2003)
49. Khaikin S E et al. *Izv. Glavn. Astron. Observat. Pulkovo* (188) 3 (1972)
50. Bogod V M et al. *Radiophys. Quantum Electron.* **47** 227 (2004); *Izv. Vyssh. Uchebn. Zaved. Radiofiz.* **47** 255 (2004)
51. Zhdanov D A, Lesovoi S V, Tokhchukova S Kh *Sol.-Terr. Phys.* **2** (2) 15 (2016); *Solnechno-Zemnaya Fiz.* **2** (2) 12 (2016)
52. Scherrer P H et al. *Sol. Phys.* **162** 129 (1995)
53. Lemen J R et al. *Sol. Phys.* **275** 17 (2012)
54. Csillaghy A, Benz A O *Astron. Astrophys.* **274** 487 (1993)
55. Kosugi T, Dennis B R, Kai K *Astrophys. J.* **324** 1118 (1988)
56. Altyntsev A T et al. *Astrophys. J.* **883** (1) 38 (2019)
57. Altyntsev A T et al. *Astron. Astrophys.* **671** A30 (2023)
58. Melrose D B, Wheatland M S *Sol. Phys.* **291** 3637 (2016)
59. Allaart M A F et al. *Sol. Phys.* **130** 183 (1990)
60. Bruggmann G et al. *Astron. Astrophys.* **240** 506 (1990)
61. Ning Z et al. *Astron. Astrophys.* **437** 691 (2005)
62. Aschwanden M J, Benz A O *Astrophys. J.* **438** 997 (1995)
63. Aschwanden M J et al. *Astrophys. J.* **455** 347 (1995)
64. Ning Z, Fu Q, Lu Q *Sol. Phys.* **194** 137 (2000)
65. Altyntsev A T et al. *Astron. Astrophys.* **411** 263 (2003)
66. Meshalkina N S et al., American Astronomical Society, SPD Meeting #37, id.8.08; *Bull. Am. Astron. Soc.* **38** 231 (2006)
67. Meshalkina N S et al. *Adv. Space Res.* **41** 936 (2008)
68. Altyntsev A T et al. *Sol. Phys.* **242** 111 (2007)
69. Priest E R, Forbes T G *Astron. Astrophys. Rev.* **10** 313 (2002)
70. Meshalkina N S et al. *Sol. Phys.* **280** 537 (2012)
71. Stepanov A V *Sov. Astron.* **17** 781 (1974); *Astron. Zh.* **50** 1243 (1973)
72. Zaitsev V V, Stepanov A V *Astron. Astrophys.* **45** 135 (1975)
73. Fomichev V V, Chernov G P *Sov. Astron.* **17** 506 (1974); *Astron. Zh.* **50** 798 (1973)
74. Chernov G P *Sov. Astron.* **17** 788 (1974); *Astron. Zh.* **50** 1254 (1973)
75. Caroubalos C et al. *Astrophys. J.* **319** 503 (1987)
76. Maxwell A, Swarup G *Nature* **181** 36 (1958)
77. Kiplinger A L et al. *Astrophys. J.* **265** L99 (1983)
78. Acton L W et al. *Publ. Astron. Soc. Jpn.* **44** L71 (1992)
79. Doschek G A *Astrophys. J.* **527** 426 (1999)
80. Feldman U et al. *Astrophys. J.* **421** 843 (1994)
81. Kovalev V A, Chernov G P, Hanaoka I *Astron. Lett.* **27** 267 (2001); *Pis'ma Astron. Zh.* **27** 310 (2001)
82. Chernov G P *Space Sci. Rev.* **127** (1–4) 195 (2006)
83. Rosenberg H *Sol. Phys.* **25** 188 (1972)
84. Chiuderi C, Giachetti R, Rosenberg H *Sol. Phys.* **33** 225 (1973)
85. Zaitsev V V, Stepanov A V *Sol. Phys.* **88** 297 (1983)
86. Kuijpers J *Astron. Astrophys.* **40** 405 (1975)
87. Fomichev V V, Fainshtein S M *Sol. Phys.* **71** 385 (1981)
88. Mollwo L *Sol. Phys.* **83** 305 (1983)
89. Ledenev V G, Yan Y-H, Fu Q-J *Chinese J. Astron. Astrophys.* **1** 475 (2001)
90. Chernov G P et al. *Astron. Astrophys.* **437** 1047 (2005)
91. Altyntsev A T et al. *Astron. Astrophys.* **431** 1037 (2005)
92. Kuznetsov A A *Astron. Astrophys.* **438** 341 (2005)
93. Altyntsev A T et al. *Sol. Phys.* **273** 163 (2011)
94. Chernov G P et al. *Astron. Astrophys.* **538** A53 (2012)
95. Stepanov A, Zaitsev V, Kronshtadtov P, in *Stars: From Collapse to Collapse, Proc. of a Conf., Nizhny Arkhyz, Russia 3–7 October 2016* (Astronomical Society of the Pacific Conf. Ser., Vol. 510, Eds Yu Yu Balega et al.) (San Francisco, CA: Astronomical Society of the Pacific, 2017) p. 284
96. Zheleznyakov V V, Zaitsev V V, Zlotnik E Ya *Astron. Lett.* **38** 589 (2012); *Pis'ma Astron. Zh.* **38** 660 (2012)
97. Eilek J A, Hankins T H *J. Plasma Phys.* **82** (3) 34 (2016)
98. Lesovoi S V et al. *Sol.-Terr. Phys.* **3** (1) 3 (2017); *Solnechno-Zemnaya Fiz.* **3** (1) 3 (2017)
99. Altyntsev A T et al. *Sol.-Terr. Phys.* **6** (2) 30 (2020); *Solnechno-Zemnaya Fiz.* **6** (2) 37 (2020)
100. Bastian T et al., in *Proc. SPIE* **3357** 609 (1998)
101. Yan et al. *Earth, Moon, Planets* **104** 97 (2009)
102. Gary D E, Nita G M, Sane N, American Astronomical Society, AAS Meeting #220 id. 204.30 (2012)